Evaluation of High-Temperature Behavior of CMSX4 + Yttrium Single-Crystal Nickel-Base Superalloy

M. Marchionni, D. Goldschmidt, and M. Maldini

CMSX4 + Y, a highly strengthened rhenium-containing second-generation single-crystal nickel-base superalloy, has been studied by creep, low-cycle, and thermomechanical fatigue in the temperature range 500 to 1100 °C. The alloy exhibits good high-temperature mechanical properties that are superior or comparable to other single-crystal superalloys. Thermomechanical fatigue resistance is equivalent to low-cycle fatigue and is cycle-shape dependent. High-temperature mechanical properties have been studied using life prediction relationships that are frequently used for creep and low-cycle fatigue data evaluation. Examination of fracture surfaces revealed that fracture induced by creep damage is internal and starts from pore-initiated cracks; however, fatigue damage starts on the external surface and propagates inward in stage II mode.

Keywords

CMSX4 + Y alloy; creep; life prediction; low cycle fatigue; thermomechanical fatigue

1. Introduction

THE continually increasing efficiency, durability, and performance of aeroengines require new materials exhibiting high mechanical resistance at elevated temperature. The development of single-crystal casting processes has led to the design of new superalloys, from which components exhibiting excellent high-temperature creep and fatigue resistance can be manufactured.[1,2] In the first stages of aeroengine turbines, the life-limiting factors for blades and vanes are oxidation, creep, thermal fatigue in the airfoil, and low-cycle fatigue in the root section. To improve high-temperature properties, oxidation resistance has been successfully increased by yttrium additions, even if the temperature of incipient melting and consequently the heat treatment window is thereby reduced.[3,4]

CMSX4, a highly strengthened rhenium-containing second-generation single-crystal nickel-base alloy, was modified by adding yttrium during the casting procedure.[5] Material properties were determined by analyzing the results of creep as well as low-cycle and thermomechanical fatigue at elevated temperatures and by investigating the involved damage micromechanisms.

M. Marchionni and **M. Maldini,** CNR-ITM, Via Induno 10, 20092 Cinisello Balsamo, Milano, Italy; and **D. Goldschmidt,** MTU München GmbH, Germany.

2. Material and Experimental Techniques

The chemical composition of CMSX4 + Y is given in Table 1. The alloy was heat treated at 1290 °C/1 h + 1305 °C/6 h, then gas fast quenched to have a fully γ' solutioned structure (no coarse γ') with some residual eutectic and a small amount of incipient melting (both <1%) (Fig. 1). The incipient melting is due to a low melting point phase generated by the addition of yttrium to the base alloy. The alloy was aged at 1140 °C/4 h + 870 °C/16 h with the objective of creating well-aligned cubic γ

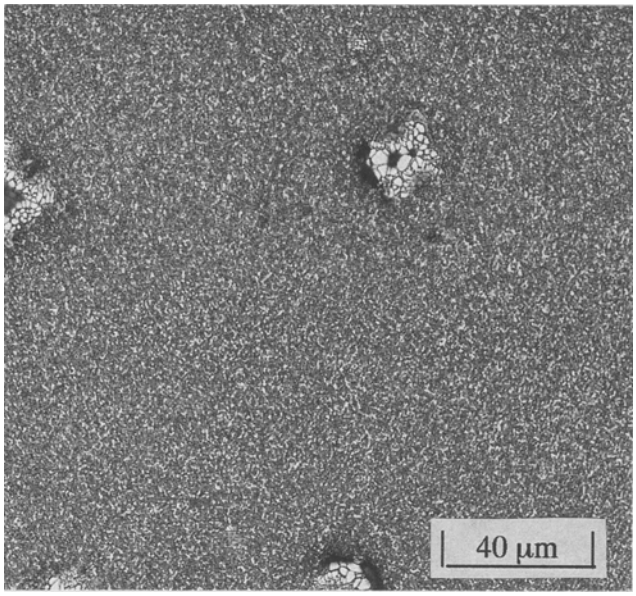

Fig. 1 Structure of CMSX4 + Y alloy showing incipient melting zones (white small areas).

Table 1 Chemical composition of CMSX4 + Y

Composition, wt%												
Ni	Co	W	Cr	Mo	Fe	Al	Ti	Ta	Hf	C	Re	Y(ppm)
60.5	9.5	6.3	6.4	0.6	0.1	5.5	0.9	6.3	0.08	0.007	2.9	50-150

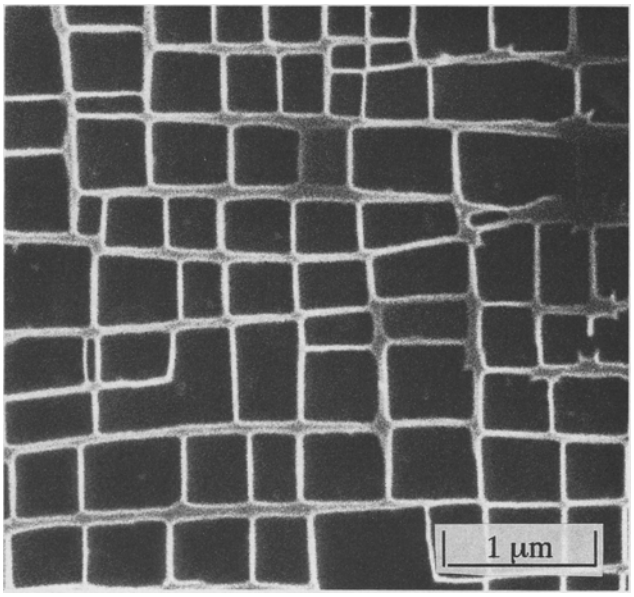

Fig. 2 Aspect of aligned γ′ particles (dark areas) in γ matrix (white lines).

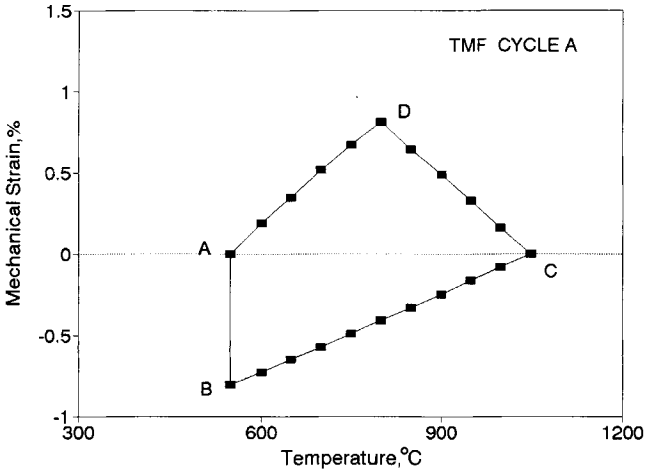

Fig. 3 Shape of thermomechanical cycle A.

′particles of about 0.5 μm in size for optimum creep strength (Fig. 2). Due to the very stable γ′ phase, the first aging temperature had to be raised by 60 °C compared to first-generation alloys (e.g., SRR99). Deviations of the ⟨001⟩ crystalline direction from the specimen axis were within 10°.

The creep specimens had a cylindrical geometry of 5.6 mm diameter and 28 mm gage length. Three thermocouples were placed in the gage length to control and monitor temperature gradients during creep. Creep strain was continuously monitored using capacitive transducers connected to extensometers that were clamped to the shoulders of the specimen. Constant-load and temperature creep tests were performed at 850 to 1050 °C and at nominal stresses selected to produce rupture times between 100 and 1500 h.

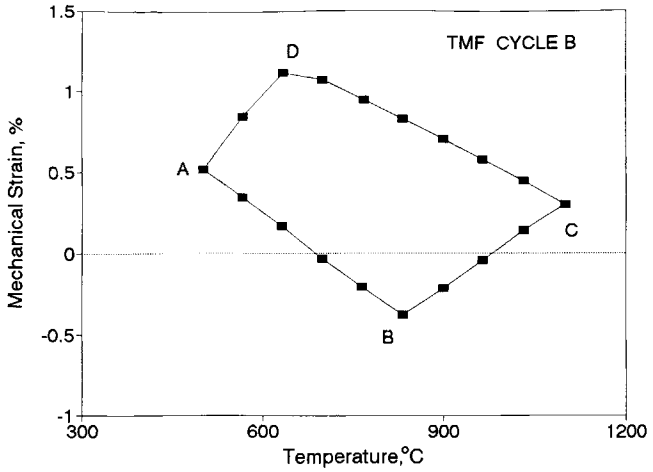

Fig. 4 Shape of thermomechanical cycle B.

The low cycle fatigue (LCF) and thermomechanical fatigue (TMF) specimens were cylindrical with a diameter of 7 mm and a gage length of 12 mm. Sample heating was achieved using an induction coil. The temperature was controlled by thermocouples that were spot welded outside the specimen gage length. The LCF tests were carried out on specimens heated by the induction coil at temperatures of 1000 and 1100 °C. The tests were performed under strain-controlled conditions at a strain rate of 3×10^{-3} s^{-1} with a triangular wave form ($R = -1$). The temperature and strain variations in the TMF tests were selected to closely model the conditions of blades in service. Figures 3 and 4 show the temperature and strain variations for cycles A (210 s) and B (180 s), respectively. During LCF and TMF tests, the stress response and the hysteresis loop were recorded at intervals.

3. Experimental Results and Discussion

3.1 *Creep Results*

CMSX4 + Y, as many complex engineering alloys of interest for high-temperature applications, exhibits a dominant accelerating creep stage, whereas primary and secondary stages are less important and sometimes negligible, both in amplitude and in duration. Such behavior is better displayed in a plot of strain rate versus strain (Fig. 5), where a linear dependence of the strain rate on the strain is manifested up to 7 to 8%.

It should be emphasized that such a strain is reached after about 80 to 90% of the specimen creep life. The final fracture mechanisms (e.g., crack propagation and/or localized reduction of area) appear to provide an extra contribution of strain rate only at the end of the creep curve. Equivalent behavior has been found in other single-crystal superalloys.[6,7] In Fig. 6, the Larson-Miller parameter versus stress of CMSX4 + Y is compared with that of SRR99, a typical first-generation single-crystal alloy. The superior creep performance of CMSX4 + Y is evident.

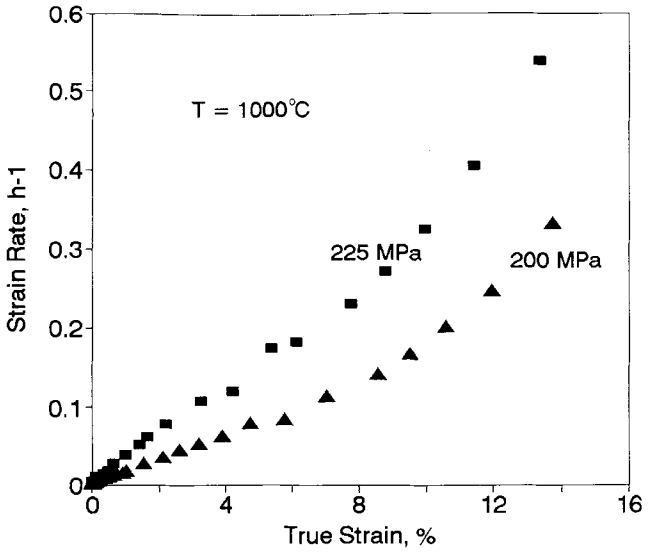

Fig. 5 Relationship between strain rate and strain at different stresses.

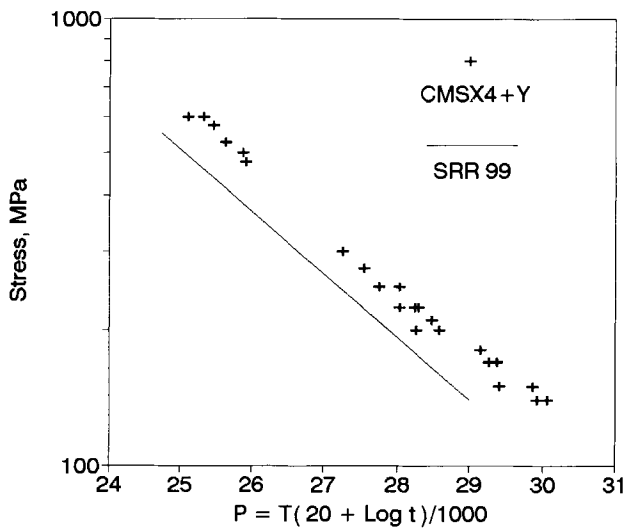

Fig. 6 Comparison of Larson-Miller plots of CMSX4 + Y and SRR99 alloys at different temperatures.

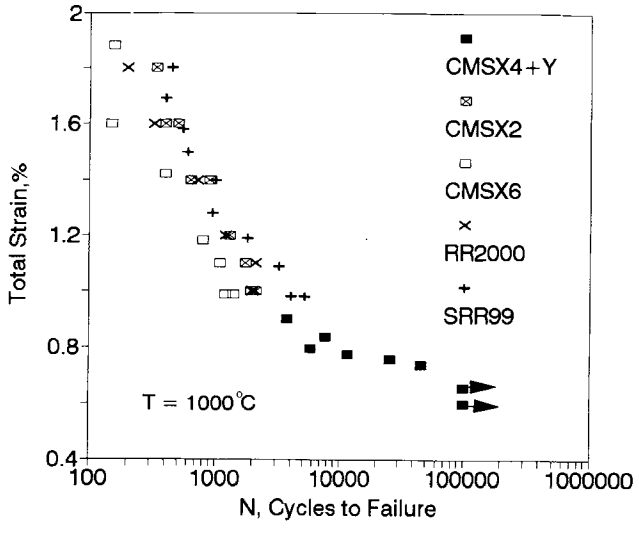

Fig. 7 Comparison of LCF lives for different single-crystal alloys.

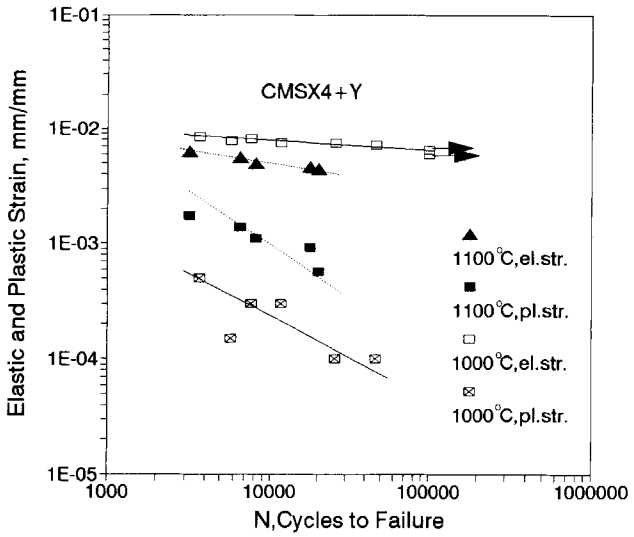

Fig. 8 Elastic and plastic strain components versus cycles to failure.

3.2 *LCF Results*

The LCF curves of CMSX4 + Y tested at 1000 °C plotted as total strain versus number of cycles to failure are shown in Fig. 7. Comparison of several single-crystal alloys at 1000 °C[8-10] reveals a fatigue life of CMSX4 + Y alloy comparable to SRR99 single crystal, but higher than other single-crystal alloys.

The plots of elastic and plastic strain components versus number of cycles to failure at 1000 and 1100 °C are reported in Fig. 8. For the total strain imposed, the plastic strain components are significantly lower than the corresponding elastic ones, due to the low Young's modulus in the ⟨001⟩ direction, which significantly reduces the plastic zone in the hysteresis loop. This characteristic increases the fatigue life compared to other polycrystal nickel-base superalloys.[10] The fatigue parameters are calculated according to the following Basquin,[11] Coffin-Manson,[12] and Ostergren[13] relationships:

$$\Delta\varepsilon_e = A \cdot N^{-\alpha} \quad [1]$$

$$\Delta\varepsilon_p = B \cdot N^{-\beta} \quad [2]$$

$$\Delta\varepsilon_p\sigma_t = D \cdot N^{-\delta} \quad [3]$$

where $\Delta\varepsilon_e$ and $\Delta\varepsilon_p$ are the elastic and plastic strain components, $\Delta\varepsilon_e$, $\Delta\varepsilon_p$, σ_t evaluated at halflife, σ_t is the tensile stress response, all calculated at half life; N is the number of cycles to

Table 2 Fatigue parameters of Eq 1, 2, and 3

Temperature, °C	*A*	α	*B*	β	*D*	δ
1000	0.017	0.093	0.023	0.40	32.9	0.67
1100	0.028	0.19	0.12	0.52	117.0	0.695

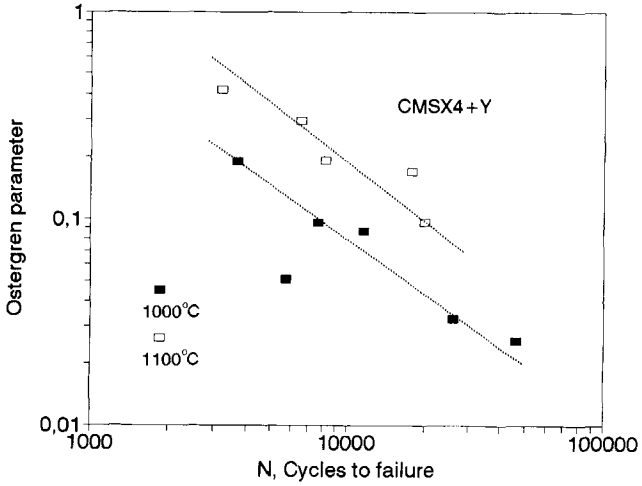

Fig. 9 Ostergren parameters versus cycles to failure.

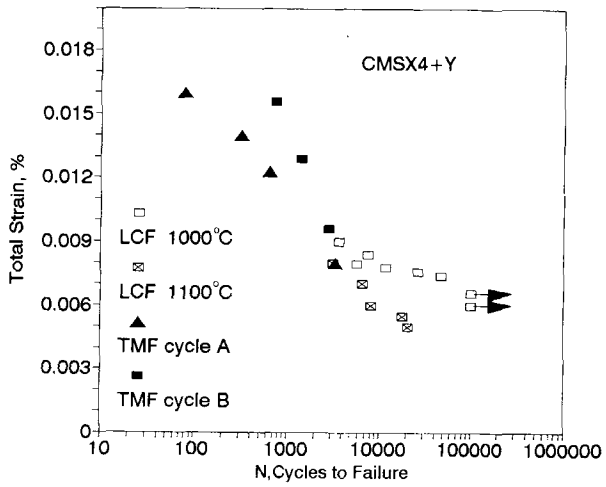

Fig. 10 Comparison of LCF and TMF endurances.

failure; and A, α, B, β, D, and δ are material constants. The values of the constants are given in Table 2.

The plots of Ostergren parameters versus number of cycles to failure are shown in Fig. 9. The curves confirm the life prediction behavior as described in the Coffin-Manson relationship. The influence of test temperature is shown in Fig. 10. Higher temperature reduces the fatigue life mainly at low strains.

3.3 *TMF Results*

The TMF results are compared to the LCF curves in Fig. 10. Cycle A in Fig. 3 was selected to obtain a symmetrical strain

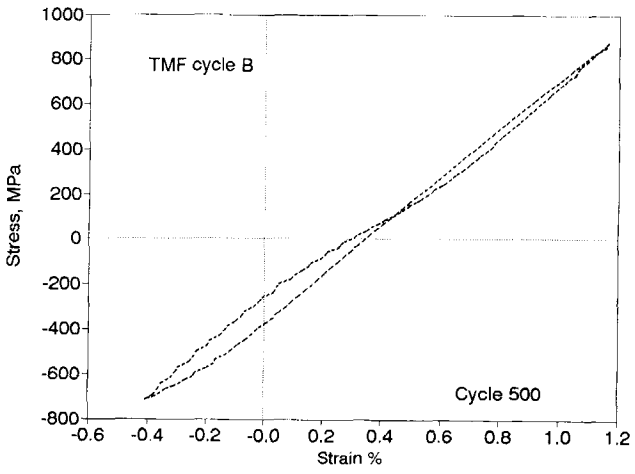

Fig. 11 Example of TMF hysteresis loop. Cycle B, $\Delta\varepsilon_m$ = 1.56%, N = 740.

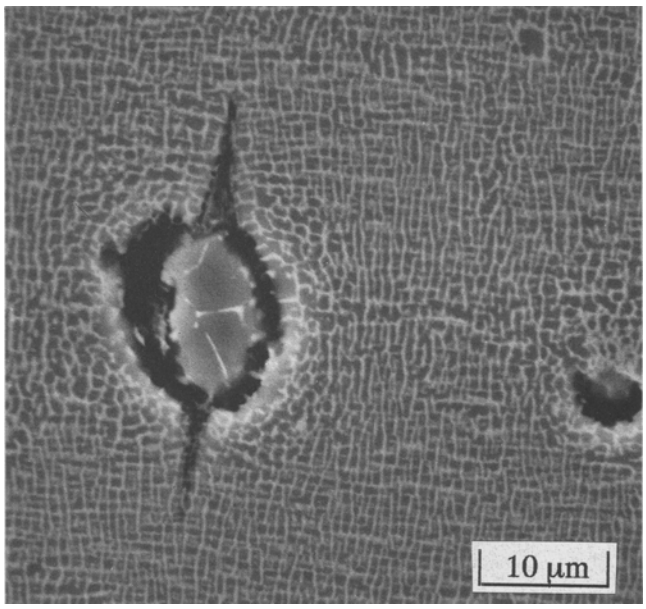

Fig. 12 Example of pore crack initiation. T = 950 °C, 225 MPa, 841 h.

variation similar to that experienced in LCF tests, whereas cycle B in Fig. 4 was found to represent variation observed in service. Because simulation of the actual strain-temperature cycle of the operational component is too time-consuming, the diamond-shape cycle B was chosen with the maximum (1100 °C) and minimum (500 °C) temperatures typical of component

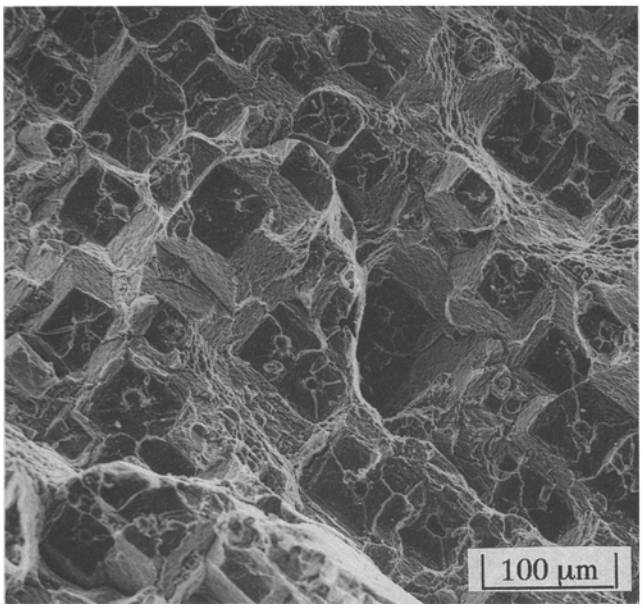

Fig. 13 Creep fracture surface aspect. Square-like facets are visible. T = 850 °C, 600 MPa, 227 h.

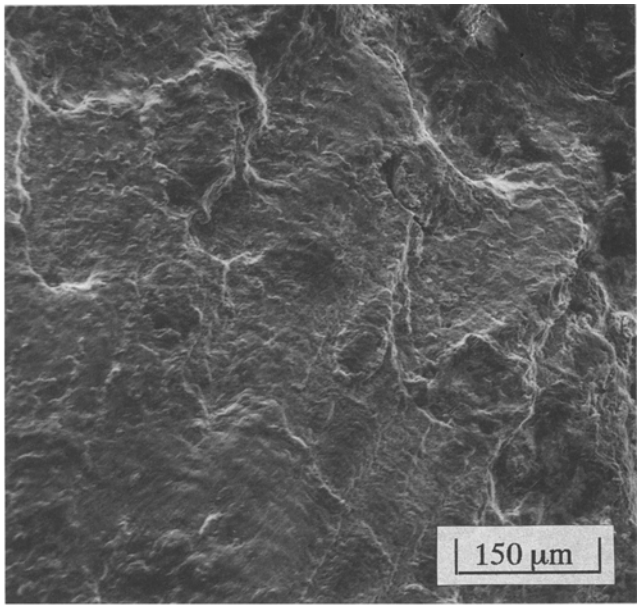

Fig. 15 Fatigue striations covered by a thick oxide layer in same specimen as Fig. 15.

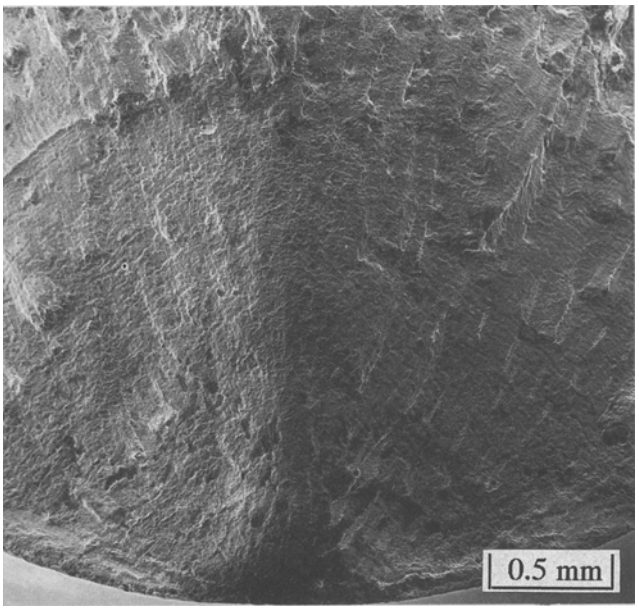

Fig. 14 Example of LCF fracture surface. T = 1100 °C, $\Delta\varepsilon_t$ = 0.8%, N = 3.200.

application, but with applied cyclic strains higher than those indicated by the component stress analysis results.

The number of cycles to failure observed in TMF tests with cycle A is comparable to that observed in low-cycle fatigue tests at the highest temperature and indicates that fatigue damage is equivalent in both cases. When cycle B is applied, the fatigue life increases moderately, probably due to the maximum tensile strain that occurs at a temperature 200 °C lower than that corresponding to the maximum tensile strain of cycle A. In this case, fatigue life prediction using only LCF results could be too conservative. An example of the hysteresis loop using cycle B is shown in Fig. 11.

3.4 *Metallography*

The creep fracture surfaces and longitudinal sections of creep-deformed specimens were examined using scanning electron microscopy (SEM). As found in other single-crystal nickel-base superalloys,[14,15] creep cracks almost always initiate at casting pores located between dendrite arms and slowly propagate anisotropically along planes perpendicular to the applied stress (Fig. 12). Figure 13 shows the morphology of creep fracture surfaces. At the lowest temperatures, they consist mainly of square-like facets oriented on (001) planes, whereas at increasing temperature the facets become progressively rounded. Metallographic measurements of crystalline orientation showed that the four edges of the facets were the ⟨110⟩ and ⟨1$\bar{1}$0⟩ directions. This creep crack behavior is consistent with the fractography of CMSX2, SRR99, and RR2000.[15]

The LCF and TMF fractures also were observed using SEM. Generally, the crack (or cracks) nucleates on the external surface of the specimen and propagates inward in stage II mode. The morphology of fracture surfaces after TMF is similar to that after LCF even if the time per cycle is quite different. An example of LCF crack initiation and propagation is shown in Fig. 14. Fracture surface fatigue striations occur inward. They are less visible at 1100 °C due to the presence of a thick oxide layer (Fig. 15). Striations also have been found in specimens fractured by TMF testing (Fig. 16), and the fracture exhibits a less pronounced oxidation layer. In the current experiments, crack initiation in LCF and TMF was always external, except for a TMF specimen tested at very low strain for 3348 cycles

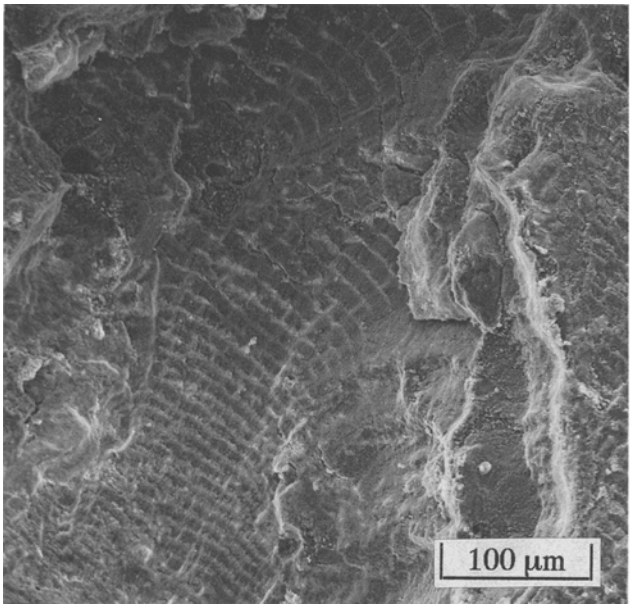

Fig. 16 Example of fatigue striations after TMF. Cycle B, $\Delta\varepsilon_m$ = 1.28%, N = 1420.

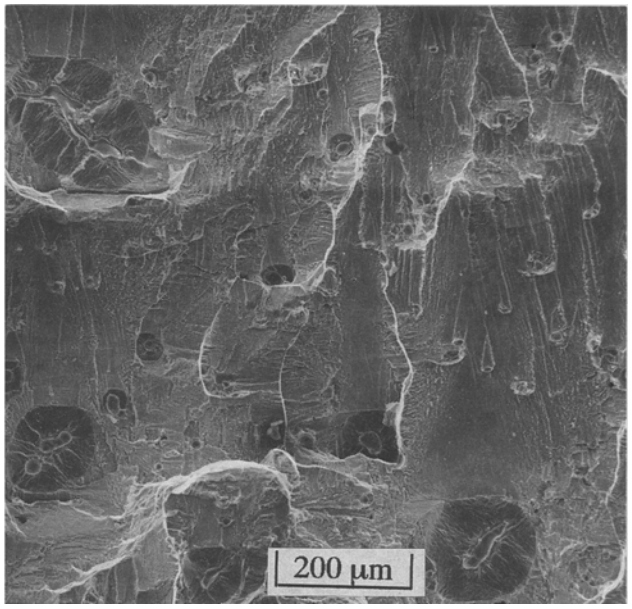

Fig. 17 Example of pore-derived cracks after TMF. Cycle A, $\Delta\varepsilon_m$ = 0.8% for n = 3348, then $\Delta\varepsilon_m$ = 1.60%, N = 90.

and then subjected to higher strain for 80 cycles until fracture occurred. In the fracture surface, secondary cracks initiated from internal pores can be observed (Fig. 17).

4. Concluding Remarks

Creep, LCF, and TMF testing on single-crystal CMSX4 + Y at different temperatures reveals that the alloy exhibits comparable or better high-temperature mechanical properties than other single-crystal nickel-base superalloys. The TMF tests performed with cycle A and LCF tests performed at 1100 °C exhibit comparable endurance whereas TMF tests performed with cycle B exhibit better fatigue life.

Creep fractures initiate from internal pores only at the last few percent of creep life, and cracks consist mainly of square-like facets oriented on ⟨001⟩ planes.

The application of LCF relationships show a good correlation between experimental data and predicted values. The LCF and TMF fractures start on the outside and propagate inward in stage II mode with the presence of fatigue striations, whereas the TMF fractures obtained at low strains exhibit the presence of internal secondary cracks initiating from pores similar to those observed in creep-deformed specimens.

Acknowledgments

The authors gratefully acknowledge Mr. E. Picco, Mr. D. Ranucci, Mr. E. Signorelli, Mr. D. Valenti of ITM, and Mr. F. Zarda of MTU for their experimental work. This project was performed as a part of European Concerted Action Cost 501 second round program.

References

1. K. Harris, G.L. Erickson, and R.E. Schwer, Development of the CMSX* Series of Single Crystal Alloys for Advanced Technology Turbine Components, in *Novel Techniques in Metal Deformation Testing*, R.H. Wagoner, Ed., Metal Society of AIME, 1983
2. K. Harris, G.L. Erickson, and R.E. Schwer, CMSX Single Crystal, CMDS & Integral Wheel Alloys Properties & Performance, *High Temperature Materials for Power Engineering 1986*, Vol I, Cost 50/501 Conf., W. Betz, R. Brunetaud, D. Coutsouradis, H. Fischmeister, T.B. Gibbons, I. Kvernes, Y. Lindblom, J.B. Marriott, and D.B. Meadowcroft, Ed., Liège, D. Reidel Publishing Company, Dordrecht Holland, 1986, p 709-728
3. P. Hupfer, Spurenelemente in Superlegierungen, *Fachberichte Hüttenpraxis Metallweiterverarbetung*, Vol 24 (No. 9), 1989, p 773
4. F.D. Hondros, *The Magic of Active Elements in the Oxidation Behavior of High Temperature Metals and Alloys*, Vol 11, E. Lang, Ed., Petten, 1989
5. F. Meyer-Olbersleben, *Thermal Fatigue of Yttrium-Modified Single Crystal Superalloys, Low Cycle Fatigue and Elasto-Plastic Behavior of Materials*, Vol 3, K.T. Rie, Ed., Elsevier Applied Science, 1992
6. M. Maldini and V. Lupinc, A Representation of Testing Creep Behavior in a Single-Crystal Nickel-Based Superalloy, *Scr. Metall.*, Vol 22, 1988, p 1737
7. V. Lupinc, M. Maldini, and V. Catena, Creep Equations of a Single Crystal Superalloy at 750-950 °C, *Evolution of Advanced Materials*, AIM/ASM, 1989, p 161
8. V. Lupinc, M. Marchionni, A.Di Gianfrancesco, U. Franzoni, V. Catena, *Nuove Superleghe a Struttura Diaxionale per Palette di Turbine a Gas Avenzate*, La Metallurgia Italiana, Vol. 81, No. 10, 1989, p 825
9. M. Marchionni, D. Ranucci, E. Picco, and D. Valenti, *Fatica Oligociclica ad Elevata Temperatura di una Superlega di Nichel Monocristallina Tipo CMSX2*, Proc. of XVIII Convegno Nazionale AIAS, Amalfi, 1990, p 571
10. M. Marchionni, V. Catena, E. Picco, and D. Ranucci, High Temperature Low Cycle Fatigue of Single Crystal Nickel Base Super-

alloys, *Proc. Fatigue '90 Int. Conf.*, H. Kitagawa and T. Tanaka, Ed., MCEP Publisher, Honolulu, 1990, p 1735-1740

11. O.H. Basquin, The Exponential Law of Endurance Tests, *Proc. ASTM*, Vol 10, 1910, p 625
12. L.F. Coffin, Jr., *Fatigue at High Temperature*, ASTM STP 520, 1972, p 12
13. W. Ostergren, A Damage Function and Associated Failure Equations for Predicting Hold Time and Frequency Effects in Elevated Temperature, Low Cycle Fatigue, *J. Test. Eval.*, Vol 4 (No. 5), 1976, p 327-339
14. A.A. Hopgood and J.W. Martin, The Creep Behaviour of Nickel-Based Single Crystal Superalloys, *Mater. Sci. Eng.*, Vol 82, 1989, p 27-36
15. S.H. Ai, V. Lupinc, and M. Maldini, Creep Fracture Mechanisms in Single Crystal Superalloys, *Scr. Metall.*, Vol 26, 1992, p 579